Electronic Supplementary Material (ESI) for Physical Chemistry Chemical Physics.

Nickel-Silver Alloy Electrocatalysts for Hydrogen Oxidation and Evolution in Alkaline Electrolyte: Supporting Information

Electrochemical testing on quartz samples

Electrochemical tests were conducted in 0.1 M KOH (Sigma) using a rotating disk electrode (RDE) set-up (Pine Instruments) and three-electrode potentiostat (Biologic Instruments) with 85% compensation for ohmic resistance. A corrosion-resistant quartz cell (Pine) was used to reduce contamination from glass etching in KOH [1]. All potentials were measured with respect to a mercury/mercuric oxide reference electrode (1.0 M KOH, Koslow Scientific), which was separated from the main cell by a potassium nitrate salt bridge. The reference electrode was calibrated to -0.869 V versus the reversible hydrogen electrode (RHE) using a commercial carbon-supported Pt catalyst. Calibrations were performed after measuring NiAg activity, and the electrolyte was refreshed before each sample. The counter-electrode was nickel wire (Alfa, 99.99%) shaped into a ring around the outer edge of the cell. This configuration was found to provide a more uniform current distribution and avoid error from sample orientation. Although heat treatment of the glassy carbon disks improved catalyst-substrate adhesion, catalyst delamination still occurred during extended periods of hydrogen bubble evolution. Longer stability tests were conducted on quartz substrates with better adhesion properties. To prepare the rectangular quartz samples, copper tape and silver paint (Ted Pella) were used to contact the electrode surface to a plastic-coated wire. The junction was then sealed in epoxy. The surface area of each electrode was determined using ImageJ. The resulting samples were attached to the RDE shaft and mounted vertically in the cell. Removing hydrogen bubbles from the electrode during HER required both rotating the electrode at 200 rpm and agitating the solution with a magnetic stirbar.

Stability testing of alloys.

Because of the thermodynamic insolubility of Ag and Ni, segregation and deactivation during device operation is a concern. As a stability test, catalysts were activated and held at -300 mV for two hours. Current vs. time is shown in Fig. 1(a), demonstrating rapid deactivation for both samples, but no change in the activity relative to each other. The electrode was then cycled between -300 mV and +200 mV. These CVs are shown on Ni in Fig. 1(b). The increase in current from the first (dashed lines) to the second cycle (solid lines) shows that some of the catalyst deactivation is reversible. Possible mechanisms of performance loss are hydride formation and removal, or specific adsorption and site blockage from electrolyte impurities [2, 3, 4]. XRD diffractograms of Ni and $Ni_{0.75}Ag_{0.25}$ before and after HER and HOR testing are shown in Fig. 2. Curves are normalized to the background intensity of the quartz substrate at $2\theta = 27°$. The alloyed Ni(111) peak remains at 44.15° before and after testing, demonstrating that electrochemical cycling does not immediately dealloy Ni and Ag. However, the Ag(111) decreases in intensity ($Ni_{0.75}Ag_{0.25}$) and the Ti(002) disappears completely (Ni) after testing. Both samples show a new peak at approximately $2\theta = 34.3°$. This peak does not correspond to any of the orientations of metallic Ni, Ag, or Ti, and is not easily assigned to any of their oxides; it may correspond to a lattice expansion of the Ti adhesion layer due to hydrogen intercalation.

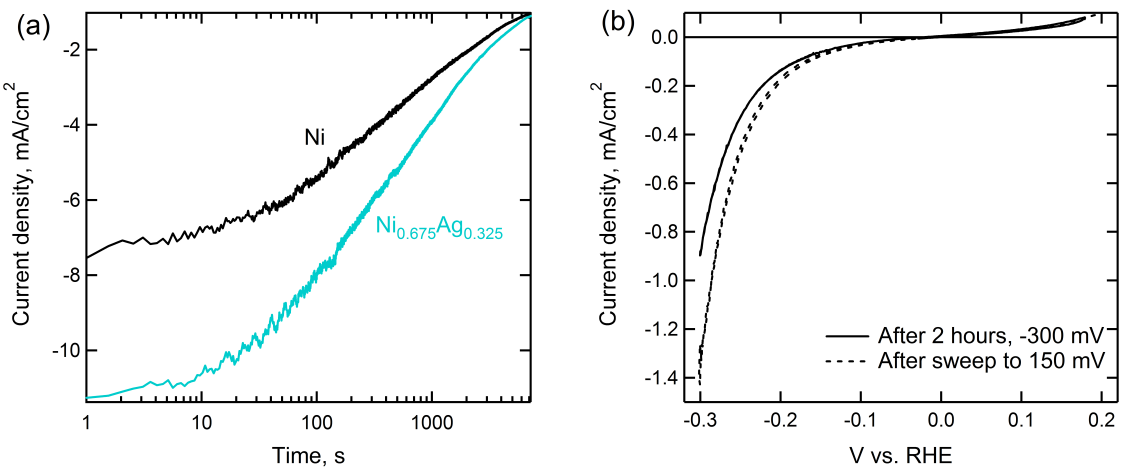

Figure 1: (a)Chronoamperometry data at -300 mV for Ni and $Ni_{0.675}Ag_{0.325}$. Both catalysts deactivate rapidly, but the difference in activity between the two samples remains relatively constant. (b) CVs after stability test at -300 mV. Cycling the electrode to +200 mV partially restores the surface activity for the catalysts, as demonstrated by the difference between the first (solid line) and second (dashed line) cycles. Substrate is quartz, and rotation speed is 200 rpm.

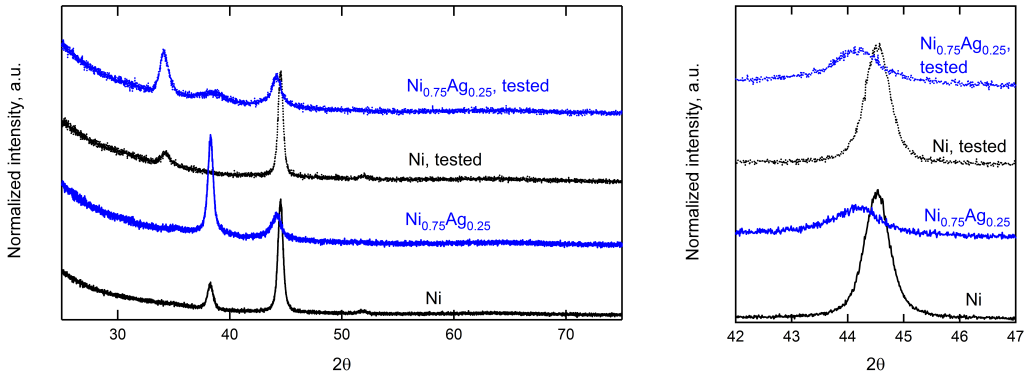

Figure 2: XRD before and after stability testing. The shift of the Ni(111) reflection (magnified at right) shows that electrochemical testing does not dealloy the AgNi sample.

High-resolution X-ray photoelectron spectroscopy

Fig. 3 shows high-resolution Ni2p scans of selected samples before and after testing. Reference spectra for NiO, $Ni(OH)_2$, and metallic Ni are also shown. The sharp peak at 853

eV in the samples before electrochemical testing shows the metallic nature of the films, but after testing the metaillic peak is reduced in intensity relative to the peaks of nickel oxides. It is not clear whether $Ni_{0.75}Ag_{0.25}$ is more, less, or equally oxidized than pure nickel after electrochemical testing. No Ni peaks are seen on the Ag sample after testing, suggesting that nickel leaching and redeposition is negligible. After testing, alloyed samples became enriched with Ni at the surface. While the surface enrichment of Ni was qualitatively consistent, the amount of Ni enrichment varied quantitatively. Both elements remained present at the surface.

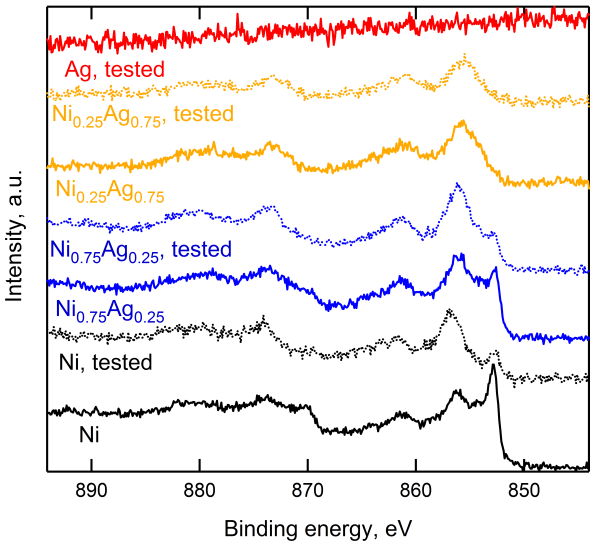

Figure 3: High-resolution XPS scans of selected samples before and after HER/HOR testing.

X-ray diffraction fitting results

Data processing and peak fitting was completed using Matlab software. First, intensity was normalized to that of the quartz substrate at $2\theta = 35°$, and the diffraction pattern of a blank quartz substrate was substracted from the measured curves. Next, the intensity of the Ti(002) peak, as measured on the pure Ni sample between 35° and 41°, was subtracted from the intensity of all Ag-containing samples. The remaining intensity was then fit with one Gaussian for the Ag(111) region from 35-51° and one for the Ni (111) from 42-26°. Initial measurements, Ti-corrected curves, and fits to the data are shown in Fig. 4. While a single Gaussian describes the Ni(111) peak well, the Ag(111) is less well approximated, especially for intermediate alloy concentrations. The d-spacing as calculated by the peak location and the grain size as calculated by the FWHM are shown in Fig. 5.

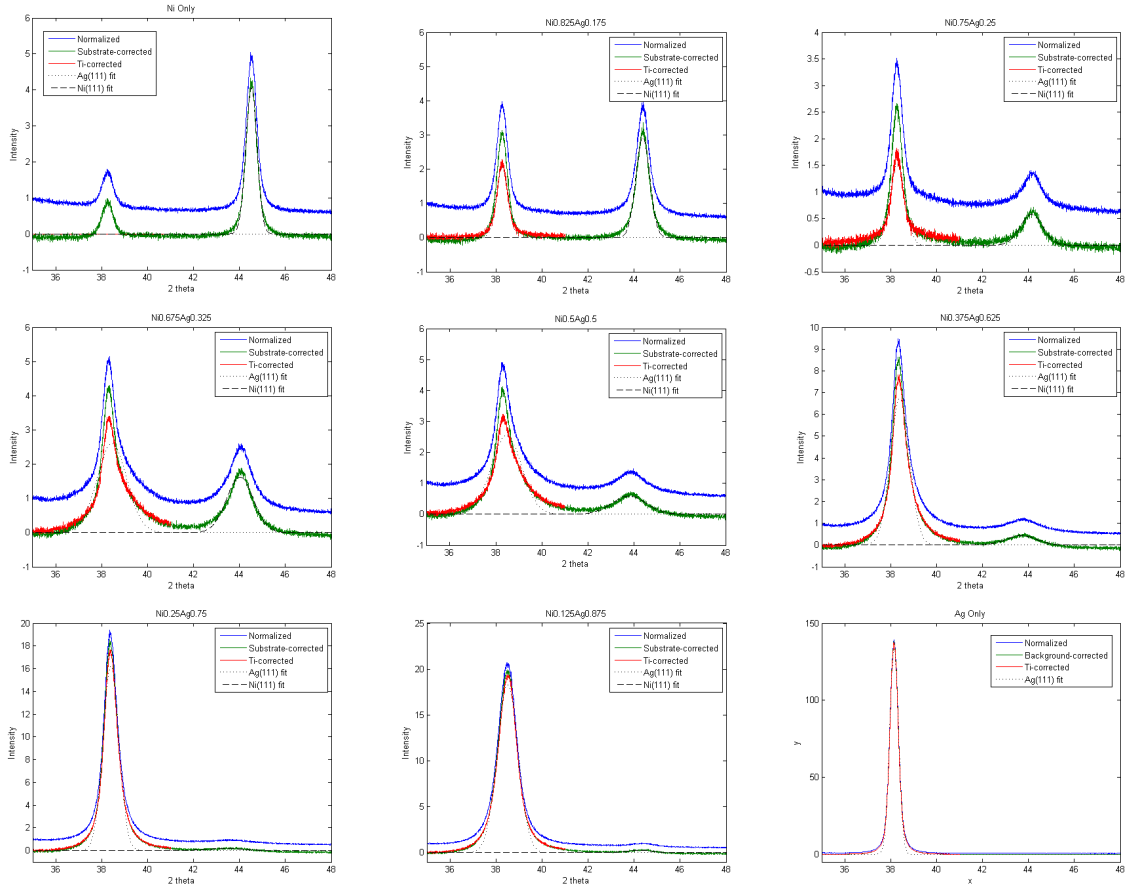

Figure 4: Normalized, corrected, and fitted data for XRD measurements on quartz.

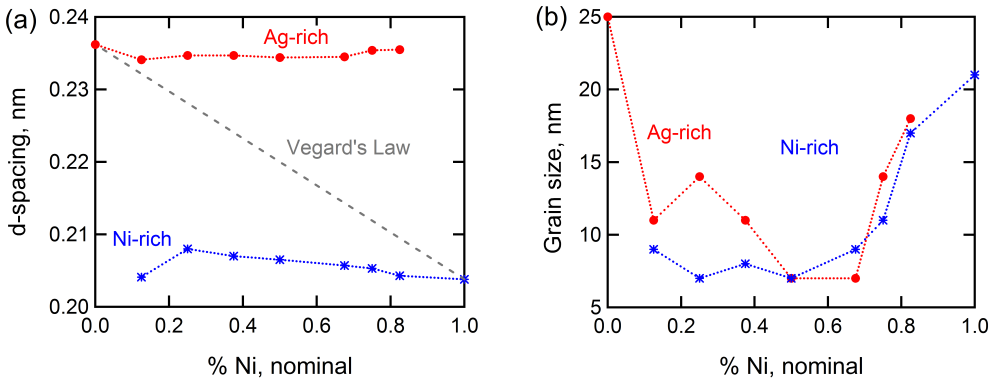

Figure 5: (a) Lattice constant and (b) grain size for the Ag-rich and Ni-rich phases, as calculated by the results of fitting the x-ray diffractograms.

OH adsorption measurements of NiAg alloys

Previous authors have reported coulometric measurement of Ni + 2 OH^- $\rightarrow$ $Ni(OH)_2 + 2e^-$ as a measurement of electrochemically active Ni surface area ($ECSA_{Ni}$)[5, 6]. However, other studies have found that the formation of hydroxide is both surface- and time-dependent [7, 8]. Despite the uncertainty of the OH-adsorption method, the charge associated with $Ni(OH)_2$ formation was measured for the samples at 50 mV/s in a N_2 atmosphere (Fig. 6). The expected charge for one monolayer of $Ni(OH)_2$ is 514 $\mu C/cm^2$. The pure Ag samples exhibited oxidation charge of approximately 137$\mu C/cm^2$; this value was attributed to double-layer capacitance and subtracted from the other measurements. The conversion yielded a $ECSA_{Ni}$: geometric area ratio of approximately 0.25 to 3. The measured $ECSA_{Ni}$ increased monotonically with nominal Ni concentration. The results of this method indicate that the NiAg alloys have less Ni surface area than pure Ni, as expected. Also shown in Fig. 6 is the identical procedure on a polycrystalline Ni disk (Pine), which was found by AFM to have a roughness factor similarly close to unity. The difference in calculated roughness between the electron-beam-deposited Ni and pc-Ni agree with a previous recommendation that OH-adsorption is at best suitable only for qualitative estimates of the $ECSA_{Ni}$ [9].

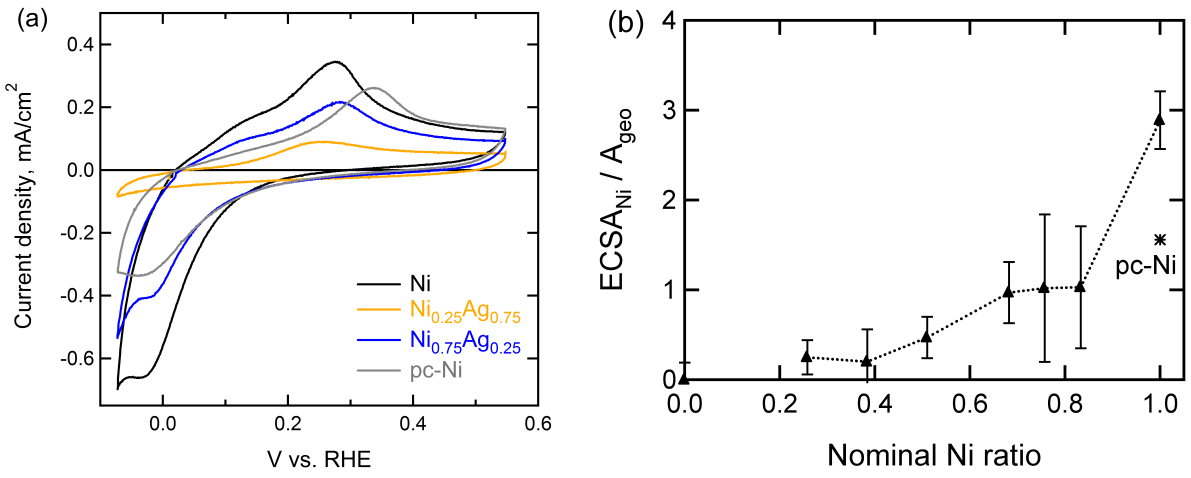

Figure 6: (a) Measurements of $Ni(OH)_2$ adsorption at 900 rpm and 50 mV/s in N_2-saturated 0.1 M KOH. (b) Calculated $ECSA_{Ni}$.

The CV represented in Fig. S6a was repeated for several cycles. The charge associated with OH adsorption decreased slightly on the second cycle and then remained constant, suggesting that surface roughening did not occur. AFM measurements after electrochemical testing also showed minimal changes to the surface morphology. (Fig. 8).

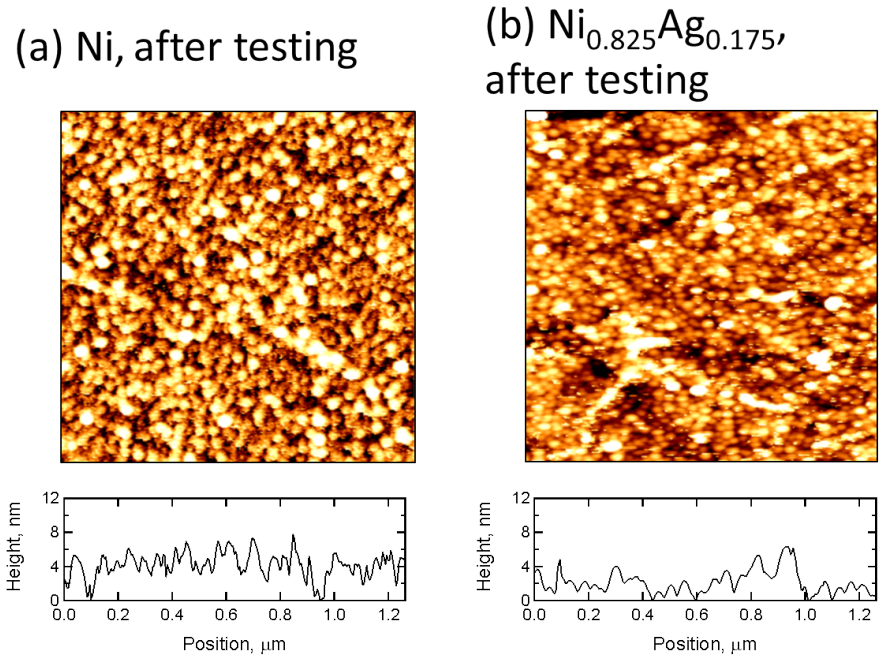

Figure 7: AFM images and line scans of Ni and $Ni_{0.825}Ag_{0.375}$ on glassy carbon after electrochemical testing. The roughness factors measured by AFM are approximately 1.03 and 1.02, respectively.

Auger electron spectroscopy map of NiAg alloy

To determine the uniformity of the NiAg alloys, local concentrations of Ni and Ag were mapped using Auger electron spectroscopy AES. An SEM image of the $Ni_{0.5}Ag_{0.5}$ alloy, along with heat maps of Ni and Ag, are shown in Fig. S7. The black spot in the SEM image is a scratch from handling the samples and provides a useful focus point on otherwise flat films. The elemental heat maps show uniform distribution of the elements, except where the scratch has removed the alloy layer and exposed the underlying Ag that was deposited during calibration. Such uniformity is expected; although the XRD data in Fig. S5 indicates that the alloys segregate into Ni-rich and Ag-rich phases, the XRD analysis also indicates that the grains are 10-20 nm large (Fig S5), which are below the resolution of this AES instrument.

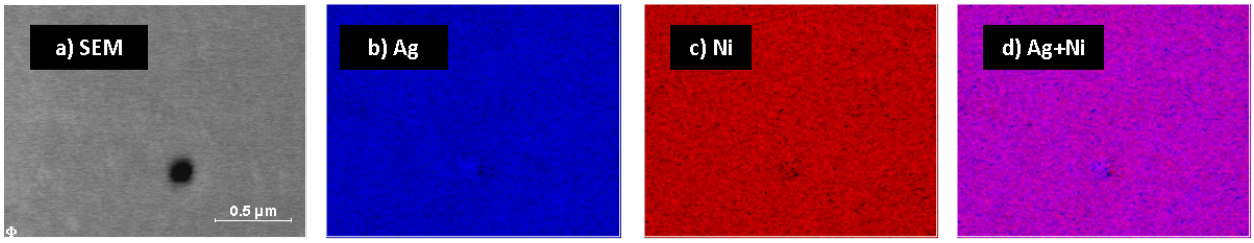

Figure 8: AES images showing a) SEM b) Ni intensity c) Ag intensity and d) combined Ni and Ag. The elements are distributed uniformly.

References

1. Mayrhofer, K. J. J., Wiberg, G. K. H. & Arenz, M. Impact of Glass Corrosion on the Electrocatalysis on Pt Electrodes in Alkaline Electrolyte. *Journal of The Electrochemical Society* **155,** P1. ISSN: 00134651 (2008).

2. Rommal, H. E. G. Time-Dependent Energy Efficiency Losses at Nickel Cathodes in Alkaline Water Electrolysis Systems. *Journal of The Electrochemical Society* **132,** 325. ISSN: 00134651 (1985).

3. Rommal, H. E. G. The Role of Absorbed Hydrogen on the Voltage-Time Behavior of Nickel Cathodes in Hydrogen Evolution. *Journal of The Electrochemical Society* **135,** 343. ISSN: 00134651 (1988).

4. Soares, D., Teschke, O & Torriani, I. Hydride effect on the kinetics of the hydrogen evolution reaction on nickel cathodes in alkaline media. *Journal of the Electrochemical Society* **139,** 98–105 (1992).

5. Machado, S. & Avaca, L. The hydrogen evolution reaction on nickel surfaces stabilized by H-absorption. *Electrochimica Acta* **39,** 1385–1391. ISSN: 00134686 (July 1994).

6. Sheng, W., Myint, M., Chen, J. G. & Yan, Y. Correlating Hydrogen Evolution Reaction Activity in Alkaline Electrolyte to Hydrogen Binding Energy on Monometallic Surfaces. *Energy & Environmental Science* **6,** 1509–1512 (2013).

7. Floner, D, Lamy, C & Leger, J. Electrocatalytic oxidation of hydrogen on polycrystal and single-crystal nickel electrodes. *Surface Science* **234,** 87–97 (1990).

8. Weininger, J. L. & Breiter, M. W. Effect of Crystal Structure on the Anodic Oxidation of Nickel. *Journal of The Electrochemical Society* **110,** 484. ISSN: 00134651 (1963).

9. Hall, D. S., Bock, C. & MacDougall, B. R. The Electrochemistry of Metallic Nickel: Oxides, Hydroxides, Hydrides and Alkaline Hydrogen Evolution. *Journal of the Electrochemical Society* **160,** F235–F243. ISSN: 0013-4651 (Jan. 2013).